ADVANCED MATERIALS

www.advmat.de

Electron Correlations Engineer Catalytic Activity of Pyrochlore Iridates for Acidic Water Oxidation

Chunyan Shang, Cong Cao, Dayou Yu, Yu Yan, Yitao Lin, Hongliang Li, Tingting Zheng, Xupeng Yan, Wenchao Yu, Shiming Zhou, and Jie Zeng**

The development of highly efficient oxygen-evolving catalysts compatible with powerful proton-exchange-membrane-based electrolyzers in acid environments is of prime importance for sustainable hydrogen production. In this field, understanding the role of electronic structure of catalysts on catalytic activity is essential but still lacking. Herein, a family of pyrochlore oxides $R_2Ir_2O_7$ (R = rare earth ions) is reported as acidic oxygen-evolving catalysts with superior-specific activities. More importantly, it is found that the intrinsic activity of this material significantly increases with the R ionic radius. Electronic structure studies reveal that the increased R ionic radius weakens electron correlations in these iridate oxides. This weakening induces an insulator–metal transition and an enhancement of Ir—O bond covalency, both of which promote oxygen evolution kinetics. This work demonstrates the importance of engineering the electron correlations to rationalize the catalytic activity toward water oxidation in strongly correlated transition-metal oxides.

Electrocatalytic water splitting has been widely studied as a sustainable and environmentally friendly approach for renewable energy supplement.[1–3] As an anodic reaction, water oxidation, also known as oxygen evolution reaction (OER), plays a critical role in this process due to the sluggish kinetics of four-proton-coupled charge transfer.[4,5] For water electrolysis, acidic proton exchange membrane (PEM) electrolyzers exhibit great advantages, such as low Ohmic losses, high-voltage efficiency, and high gas purity relative to alkaline electrolyzers.[4–6] Currently, iridium oxide IrO_2 is generally regarded as the optimal catalyst with a compromise between activity and stability for OER under acidic conditions.[5–7] However, it suffers from high cost and still low intrinsic activity. Usually, the specific activity, measured by normalizing the current density to the catalyst surface area, is less than 0.05 mA cm^{-2}_{oxide} at an overpotential of 300 mV (η = 300 mV) under pH 1.[5,8] Thus, developing catalysts with less content of Ir metal and higher intrinsic activity is quite appealing for acidic water oxidation.

To lower the Ir amount, many efforts have focused mainly on dispersing iridium oxides on a conductive high surface area support or by doping of nonprecious metals.[9–12] The enhanced activities have successfully reported in doped IrO_2 by various transition-metals like Ni, Co, and Cu. Several possible factors from the dopants, such as large surface active area, high coverage of reactive surface hydroxyl groups, and modified d-orbital occupation, were proposed to be involved in the enhancements.[10–12] However, the material properties determining the activity of those catalysts remain unclear. Moreover, the relatively smaller ion radii of 3d transition metals than that of Ir ion usually limit their solubility in the host structure due to lattice mismatch, which restricts a systemic study with a continuous change in the material properties.

Recently, another promising strategy has been developed to both reduce the Ir usage and promote the intrinsic activity, which is the synthesis of complex iridate oxides.[13–19] Various iridate oxides, such as perovskite- and pyrochlore-type compounds, were found to exhibit superior activities to the benchmark IrO_2 catalyst. For example, the specific activity at η = 300 mV in acidic conditions approached about 0.1 mA cm^{-2}_{oxide} for pyrochlore oxide $Y_2Ir_2O_7$ and even above 1.0 mA cm^{-2}_{oxide} for the perovskite oxide Ba_2NdIrO_6.[14,15] Despite of these achievements, still there is rare fundamental understanding of the underlying mechanism, especially the potential correlation between their catalytic activities and electronic structures, which should be essential for the design of future efficient electrocatalysts. In particular, 5d iridate oxides are a typical class of strongly correlated electron systems in which the charge, spin, orbital, and lattice degrees of freedom couple each other.[20–26] As a typical representation, pyrochlore iridate oxides $R_2Ir_2O_7$ (R = rare earth ions) have drawn intensive attention in recent years since the interplay between electron correlations and spin–orbital couplings in this material induces a fascinating electronic phase diagram including various intriguing states, such as topological Mott insulators, Wely semimetals, and spin-liquid metals.[22–26] Moreover, the states can be finely tuned by changing R ions via the modification of 5d electron correlations,[24–26] which may provide an excellent

C. Shang, C. Cao, D. Yu, Y. Yan, Y. Lin, H. Li, T. Zheng, X. Yan, W. Yu, Prof. S. Zhou, Prof. J. Zeng
Hefei National Laboratory for Physical Sciences at the Microscale
Key Laboratory of Strongly-Coupled Quantum Matter Physics of Chinese Academy of Sciences, and Department of Chemical Physics
University of Science and Technology of China
Hefei, Anhui 230026, P. R. China
E-mail: zhousm@ustc.edu.cn; zengj@ustc.edu.cn

The ORCID identification number(s) for the author(s) of this article can be found under https://doi.org/10.1002/adma.201805104.

DOI: 10.1002/adma.201805104

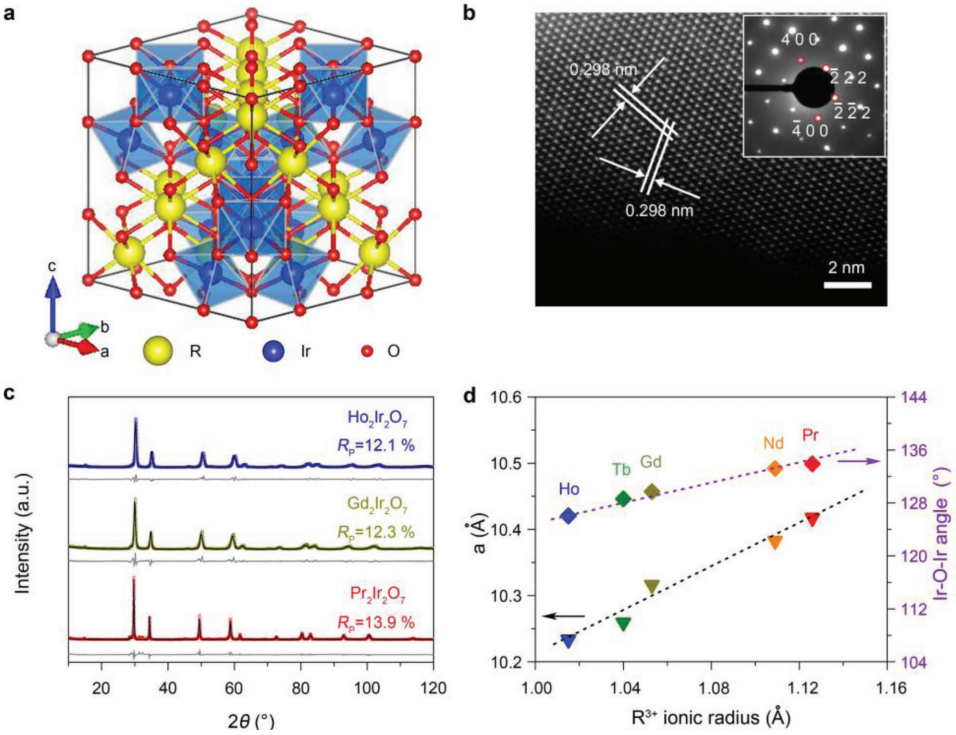

Figure 1. a) Crystal structure of $R_2Ir_2O_7$. b) HRTEM image of $Pr_2Ir_2O_7$ particles. The inset shows the corresponding SAED pattern. c) Rietveld refinements of XRD patterns of $R_2Ir_2O_7$. The colored dots, black lines, and gray lines are the experimental data, calculated data, and difference between them, respectively. R_p is the goodness-of-fit parameter obtained through Rietveld refinements. d) Ir—O—Ir bond angles and lattice constant a of $R_2Ir_2O_7$. The dotted lines guide the eye.

platform to explore the dependence of the catalytic activity on the electronic structures.

Herein, based on a family of pyrochlore oxides $R_2Ir_2O_7$ (R = rare earth ions), we demonstrate the relationship between catalytic activity and electronic correlations in iridate oxides for acidic water oxidation. We find that as the radius of R ions increases the intrinsic activity exhibits a significant enhancement. Specifically, the specific current density at η = 300 mV under pH = 1 reaches a high value of 13.3 mA cm^{-2}_{oxide} for R = Pr. Electronic structure studies reveal that this enhancement is attributed to the weakening of the effective electron correlations via chemical pressure effect, which results in a transition from insulator to metal and a large increase in the hybridization of Ir 5d–O 2p orbitals.

The polycrystalline powders of $R_2Ir_2O_7$ (R = Ho, Tb, Gd, Nd, and Pr) were prepared by a sol–gel method.[27] **Figure 1**a shows the crystal structure of pyrochlore-type $R_2Ir_2O_7$, where the R—O and Ir—O frameworks form R_2O chains and corner-shared IrO_6 octahedra, respectively (Figure S1, Supporting Information).[14,23] Based on scanning electron microscopy–energy-dispersive spectroscopy (SEM-EDS), the atomic ratio of R to Ir was determined to be 1.02, 1.04, 1.03, 1.01, and 1.01 for $Ho_2Ir_2O_7$, $Tb_2Ir_2O_7$, $Gd_2Ir_2O_7$, $Nd_2Ir_2O_7$, and $Pr_2Ir_2O_7$, respectively, consistent with the theoretical value of 1:1 (Figure S2, Supporting Information). The particle size of these samples is approximately hundreds of nanometers (Figure S3, Supporting Information). Figure 1b shows a representative high-resolution transmission electron microscopy (HRTEM) analysis and a selected area electron diffraction (SAED) pattern of $Pr_2Ir_2O_7$ particles. The interplane spacing was determined as 0.298 nm, corresponding to the (2 2 2) or (-2 -2 2) plane of face-centered cubic pyrochlore phase.[12,17] The high crystallinity and phase structure of as-prepared samples were further confirmed by X-ray diffraction (XRD) patterns (Figure 1c and Figure S4, Supporting Information), where the major reflections can be well indexed with a Fd3m space group.[14,23] Rietveld refinements on the diffraction data reveal that the lattice constant a increased with the R ionic radius (Figure 1d). For pyrochlore oxides, the lattice expansion with R ionic radius is generally attributed to the increase in Ir—O—Ir bond angle via chemical pressure effect. As plotted in Figure 1d, the refined Ir—O—Ir bond angles for our samples indeed exhibited an obvious increase with the R ionic radius. This dependence was also supported by Raman spectra (Figure S5, Supporting Information), where a blueshift of the peak around 500 cm^{-1} assigned to the bending mode of A_{1g} indicates the expansion of the Ir—O—Ir bond with the increase of the R ionic radius.[28,29]

The electrocatalytic OER properties of pyrochlore oxides $R_2Ir_2O_7$ were evaluated in O_2-saturated 0.1 M $HClO_4$ solution using a standard three-electrode system. The polarization curves for all the samples, along with the commercial IrO_2 nanoparticles as a reference, show a strong dependence of the OER activity on the type of R ions (Figure S6a, Supporting Information). As R varied from Ho to Pr, the current density was remarkably promoted. Meanwhile, the onset potential was reduced from 1.49 to 1.41 V. This promotion was also reflected

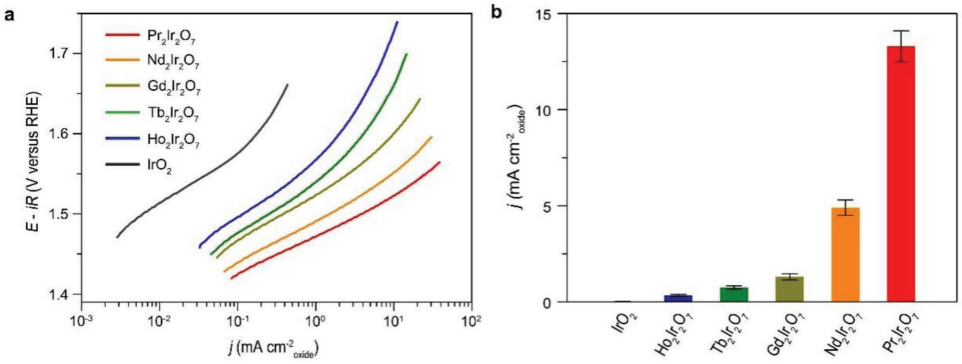

Figure 2. a) The specific OER activity of $R_2Ir_2O_7$ and IrO_2. b) Specific OER activity at $\eta = 300$ mV. Error bars represent standard deviation from at least three independent measurements.

by the mass activity, obtained by normalizing the current density to the Ir metal mass (Figure S6b, Supporting Information). All the pyrochlore iridates exhibited a higher mass activity than the commercial IrO_2 nanoparticles. Specifically, $Pr_2Ir_2O_7$ exhibited the highest mass activity of 424.5 A g^{-1}_{Ir} at η = 300 mV, which was about 21 times larger than that (20.4 A g^{-1}_{Ir}) of the commercial IrO_2 nanoparticles.

In order to address the crucial role of the R ions on the OER performance in $R_2Ir_2O_7$, the specific activity was further calculated by normalizing the mass activity with the Brunauer–Emmett–Teller surface areas (Figure S7, Supporting Information), as plotted in **Figure 2**a. With the increase of R ionic radius, a substantial improvement in the intrinsic activity was observed. The overpotential at 10 mA cm^{-2}_{oxide} decreased from about 500 to 290 mV. At η = 300 mV, the current densities (Figure 2b) approached to about 4.9 and 13.3 mA cm^{-2}_{oxide} for R = Nd and Pr, which are about 14 and 39 times higher than that of R = Ho, respectively. Similar tendency was reproduced in the normalized activity by the electrochemically active surface areas, which were estimated from the electrochemical double-layer capacitance measurements (Figures S8 and S9, Supporting Information). More interestingly, the intrinsic OER activities of all the pyrochlore iridates were much higher than the commercial IrO_2 nanoparticles. At η = 300 mV, the specific current densities for R = Ho, Tb, Gb, Nd, and Pr were about 17, 38, 65, 210, and 670 times higher than that of IrO_2, respectively. Notably, $Nd_2Ir_2O_7$ and $Pr_2Ir_2O_7$ outperformed most of the Ir-based single-phase catalysts previously reported (Table S1, Supporting Information).

To assess the electrocatalytic stability of the pyrochlore iridate oxides, a long-term OER test at 10 mA cm^{-2}_{disk} and 1000 cycles of voltammogram (Figure S10, Supporting Information) were performed for R = Nd and Pr, together with the commercial IrO_2 as comparison. The pyrochlore iridates were electrochemically stable under both the testing conditions, while the IrO_2 catalyst nearly lost its activity after 8000 s or 800 cycles. The steady of the pyrochlore iridate oxides was further supported by the XRD and HRTEM measurements on the $Pr_2Ir_2O_7$ electrode before and after the OER tests (Figure S11, Supporting Information). No detectable changes in XRD patterns were found between before and after the tests. Moreover, HRTEM images showed that the surface structure of $Pr_2Ir_2O_7$ catalyst after OER tests still maintained. Low-resolution transmission electron microscopy (TEM) characterization of near surface area of and before and after stability test showed that no visible change was found around the surface area of pyrochlore oxides, showing the acid stability of $R_2Ir_2O_7$ (Figure S12, Supporting Information). Besides, the surficial chemistry was investigated by X-ray photoelectron spectroscopy (XPS) spectra (Figure S13, Supporting Information), showing no obvious changes in the XPS spectra of Ir 4f and R 3d, indicating that the chemical state of Ir an R ions remained nearly the same with that of pristine pyrochlore oxides. In addition, we detected the electrolyte after OER test by inductively coupled plasma atomic emission spectroscopy (ICP-AES). Both the content of Ir and R were below the detection limit. Moreover, postcharacterizations by STEM-EDS and EDS mapping disclose that the atomic ratios of R to Ir for tested $Nd_2Ir_2O_7$ and $Pr_2Ir_2O_7$ are 1.03 and 1.06, which approaches to that of pristine ones which are 1.00 and 1.08 (Figure S14, Supporting Information). In this case, the atomic ratio of R to Ir remained unchanged after the reaction. Taken together, no R or Ir ions were leached out during OER reaction. These results underscore that the pyrochlore iridate oxides, especially for R = Pr, are highly active and stable catalysts for acidic water oxidation, making them a promising catalyst in commercial PEM-based water splitting electrolysis.

The electrochemical measurements clearly reveal that the intrinsic OER activity of $R_2Ir_2O_7$ strongly depends on R ions. For this strongly correlated system, it has been pointed out that the correlations among Ir 5d electrons play a vital role in their electronic properties.[22–26] Generally, the effective electron correlations are determined by the ratio of U/W, where U and W are the on-site Coulomb repulsion and the bandwidth, respectively.[24,25] The increase of Ir—O—Ir bond angle with the R ionic radius leads to a larger hopping parameter between Ir 5d electrons and hence an increased W value.[25] As a result, the effective electron correlations in $R_2Ir_2O_7$ are modified by the Ir—O—Ir bond angle via changing R ions. In order to characterize the strength of electron correlations for as-prepared pyrochlore oxides, Ir 4f XPS were carried out (**Figure 3**a and Figure S15, Supporting Information). For all the iridates, a multicomponent peak structure was observed, which can be fitted with two doublets.[30] The broad doublet at lower binding energy corresponds to an unscreened component (u) and the sharp doublet at higher binding energy to a screened one (s).[30] The relative ratio of u/s has been employed as a valid parameter to measure the

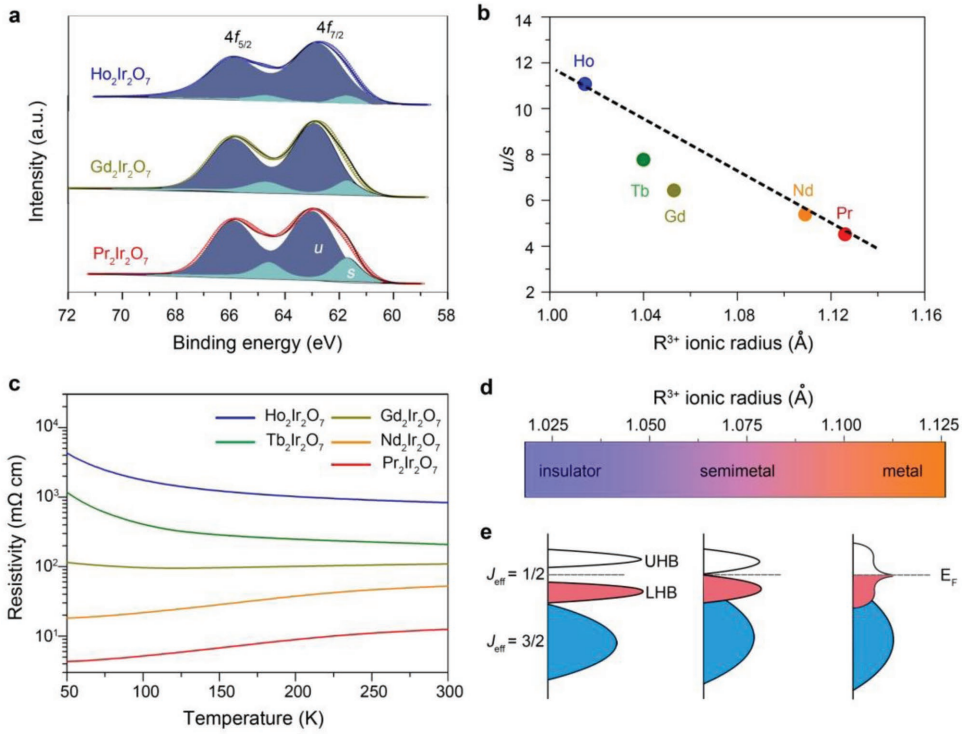

Figure 3. a) Ir 4f XPS spectra of $R_2Ir_2O_7$. b) The ratio of *u*/*s* for $R_2Ir_2O_7$. The doublet *u* and *s* correspond to the unscreened and screened 4f components, respectively. The dotted line guides the eye. c) Temperature-dependent resistivity. d,e) Electronic phase diagram around room temperature and the corresponding schematic band structures of Ir 5d orbitals.

strength of electron correlations for 4d and 5d metal oxides.[30,31] Figure 3b plots the ratios of *u*/*s* for $R_2Ir_2O_7$ with different R ions. When R varies from Ho to Pr, the ratio largely reduced from about 11.1 to 4.5, which indicates that increasing the R ionic radius weakened the electron correlations.

The electrical transport measurements were further performed to explore the electronic properties of pyrochlore iridate oxides. Figure 3c displays the temperature-dependent electrical resistivity of $R_2Ir_2O_7$. For small R ions, i. e., Ho and Tb, the resistivity increased with the decrease of the temperature, signifying a typically insulating behavior. For the moderate R ion, i. e., Gd, the resistivity exhibited a less dependence on the temperature. Moreover, the value of resistivity was around 100 mΩ cm, which approached to that of the metals. Both features suggest that $Gd_2Ir_2O_7$ behaved like a semimetal.[26] For larger R ions, i.e., Nd and Pr, the resistivity decreased upon cooling, meaning a metallic behavior. Moreover, in the entire temperature region, the resistivity monotonically decreased with the increase of R ionic radius. Specifically, at 300 K, it reduced from about 840 to 12 mΩ cm as R changed from Ho to Pr. On the basis of the transport measurements, we established an electronic phase diagram near room temperature for $R_2Ir_2O_7$. As illustrated in Figure 3d, the increase of R ionic radius induces an insulator–semimetal–metal transition.

For IrO_2, Ir^{4+} ions have no electron in e_g orbital, since all electrons are at low-spin state and in t_{2g} orbitals. For pyrochlore iridate oxides, the 5d electrons of Ir^{4+} ions under O_h symmetry in IrO_6 octahedra are split into t_{2g} and e_g orbital states by the crystal field energy, yielding a $t^5{}_{2g}$ low-spin configuration.[20] Due to the strong spin–orbit interactions, the t_{2g} band is further split up into a narrower, half-filled $J_{eff} = 1/2$ band and a wider, filled $J_{eff} = 3/2$ band.[20] The half-filled $J_{eff} = 1/2$ band shares the same merit with the single electron filled e_g orbital reported in 3d transition-metal oxides, which results in the high reactivity with absorbed oxygen. Accordingly, the higher OER activities in $R_2Ir_2O_7$ derive from the stronger spin–orbital couplings relative to IrO_2.

As for the comparison between different $R_2Ir_2O_7$, the strong electron correlations are taken into account. In this case, the $J_{eff} = 1/2$ band is further divided into an upper Hubbard band and a lower Hubbard band with a Mott gap, making it a $J_{eff} = 1/2$ Mott insulator (Figure S16, Supporting Information).[20] This feature was suitable for R = Ho and Tb due to relatively larger electron correlations, as shown in the left of Figure 3e. When the R ionic radius increased, accompanied by the decrease of electron correlations, the gap gradually reduced. For R = Gd, it was close to zero, which was associated with the semimetal state (see the middle of Figure 3e). Upon decreasing the electron correlations, as for R = Nd and Pr, the gap completely disappeared and hence the metallic behavior emerged (see the right of Figure 3e).[26] Therefore, the electronic structure of this strongly correlated system was directly controlled by the effective electron correlations via changing R ions.

For oxygen-evolving catalysts, the high conductivity could facilitate the charge transfer between catalyst–electrolyte and catalyst–support electrode interfaces, which is beneficial for the OER process.[32,33] In our case, the weakening of the electron correlations induced an insulator–semimetal–metal transition for $R_2Ir_2O_7$, accompanied by a significant enhancement

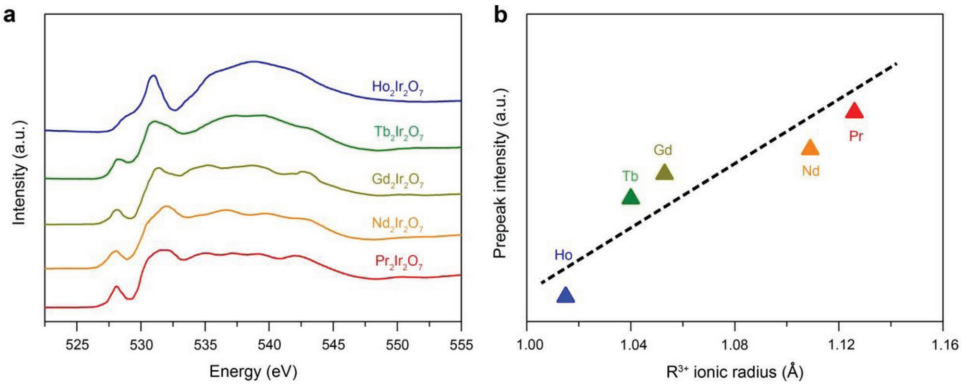

Figure 4. a,b) O K-edge XAS and the normalized intensity of the prepeak around 528 eV.

in the conductivity. Thus, it is believed that the OER kinetic was accelerated by the weakening of the electron correlations. This feature was confirmed by the electrochemical impedance spectroscopy measurements (Figure S17, Supporting Information), where the Nyquist plots revealed a gradually decrease in the charge transfer resistance with R varying from Ho to Pr. On the other hand, the covalency of metal-oxygen bonds has been recently demonstrated to play a critical role in the OER process for transition-metal oxides.[16,34–37] A higher covalency is regarded to facilitate the reaction kinetics and give rise to a higher oxygen-evolving activity. For $R_2Ir_2O_7$, the reduction in the electron correlations was associated with the broadened Ir 5d bands, which would enhance the Ir—O covalency due to the increased orbital hybridization. To evaluate the strength of metal–oxygen orbital hybridization in these oxides, O K-edge X-ray absorption spectra (XAS) were further carried out. As shown in **Figure 4**a, all the spectra present a prepeak around 528 eV, which corresponds to the transition from the O 1s core level to the unoccupied O 2p states hybridized with Ir 5d t_{2g} orbitals.[37–40] When the R ionic radius increases, the normalized intensity of the prepeak exhibits an obvious increase (Figure 4b). This result clearly supports that the Ir 5d–O 2p hybridization is enhanced by weakening the electron correlations, which benefits the oxygen redox reaction and thus boosts the water oxidation.

In summary, we develop the pyrochlore-type iridate oxides $R_2Ir_2O_7$ as highly active and stable OER catalysts for acidic water oxidation, overwhelmingly superior to the benchmark IrO_2 nanoparticles. More interestingly, the intrinsic activity exhibits a significant increase with the R ionic radius in this material. The increase of R ionic radius weakens the electron correlations via broadening the Ir 5d bandwidths, which gives rise to an insulator–metal transition and a strengthened hybridization between Ir 5d and O 2p orbitals. The promoted conductivity and enhanced covalency of Ir—O bonds improve the OER activity. This work not only provides deep insight into the role of the electron correlations in the catalytic activity, but also points toward a direction to design highly efficient oxygen-evolving catalysts in strongly correlated transition metal oxides.

Supporting Information

Supporting Information is available from the Wiley Online Library or from the author.

Acknowledgements

C.S. and C.C. contributed equally to this work. This work was supported by NSFC (U1732149 and 21573206), Key Research Program of Frontier Sciences of the CAS (QYZDB-SSW-SLH017), Anhui Provincial Key Scientific and Technological Project (1704a0902013), Major Program of Development Foundation of Hefei Center for Physical Science and Technology (2017FXZY002), and Fundamental Research Funds for the Central Universities. This work was partially carried out at the USTC Center for Micro and Nanoscale Research and Fabrication.

Conflict of Interest

The authors declare no conflict of interest.

Keywords

catalytic activity, electron correlations, iridate oxides, oxygen evolution reaction

Received: August 6, 2018
Revised: October 27, 2018
Published online: December 14, 2018

[1] M. S. Dresselhaus, I. L. Thomas, *Nature* **2001**, *414*, 332.
[2] J. A. Turner, *Science* **2004**, *305*, 972.
[3] J. H. Montoya, L. C. Seitz, P. Chakthranont, A. Vojvodic, T. F. Jaramillo, J. K. Nørskov, *Nat. Mater.* **2017**, *16*, 70.
[4] Z. W. Seh, J. Kibsgaard, C. F. Dickens, I. Chorkendorff, J. K. Nørskov, T. F. Jaramillo, *Science* **2017**, *355*, eaad4998.
[5] C. C. L. McCrory, S. Jung, I. M. Ferrer, S. M. Chatman, J. C. Peters, T. F. Jaramillo, *J. Am. Chem. Soc.* **2015**, *137*, 4347.
[6] T. Reier, H. N. Nong, D. Teschner, R. Schlögl, P. Strasser, *Adv. Energy Mater.* **2017**, *7*, 1601275.
[7] N. Danilovic, R. Subbaraman, K. C. Chang, S. H. Chang, Y. J. Kang, J. Snyder, V. R. Stamenkovic, *J. Phys. Chem. Lett.* **2014**, *5*, 2474.
[8] Y. Lee, J. Suntivich, K. J. May, E. E. Perry, Y. Shao-Horn, *J. Phys. Chem. Lett.* **2012**, *3*, 399.
[9] H. S. Oh, H. N. Nong, P. Strasser, *Adv. Funct. Mater.* **2015**, *25*, 1074.
[10] W. Hu, H. Zhong, W. Liang, S. Chen, *ACS Appl. Mater. Interfaces* **2014**, *6*, 12729.
[11] T. Reier, Z. Pawolek, S. Cherevko, M. Bruns, T. Jones, D. Teschner, K. J. Mayrhofer, *J. Am. Chem. Soc.* **2015**, *137*, 13031.

[12] W. Sun, Y. Song, X. Gong, L. Cao, J. Yang, *Chem. Sci.* **2015**, *6*, 4993.
[13] K. Sardar, S. C. Ball, J. D. Sharman, D. Thompsett, J. M. Fisher, R. A. Smith, R. I. Walton, *Chem. Mater.* **2012**, *24*, 4192.
[14] D. Lebedev, M. Povia, K. Waltar, P. M. Abdala, I. E. Castelli, E. Fabbri, T. J. Schmidt, *Chem. Mater.* **2017**, *29*, 5182.
[15] O. Diaz-Morales, S. Raaijman, R. Kortlever, P. J. Kooyman, T. Wezendonk, J. Gascon, M. T. Koper, *Nat. Commun.* **2016**, *7*, 12363.
[16] A. Grimaud, A. Demortière, M. Saubanere, W. Dachraoui, M. Duchamp, M. L. Doublet, J. M. Tarascon, *Nat. Energy* **2017**, *2*, 16189.
[17] L. C. Seitz, C. F. Dickens, K. Nishio, Y. Hikita, J. Montoya, A. Doyle, T. F. Jaramillo, *Science* **2016**, *353*, 1011.
[18] D. Lebedev, M. Povia, K. Waltar, P. M. Abdala, I. E. Castelli, E. Fabbri, M. V. Blanco, A. Fedorov, C. Copéret, N. Marzari, T. J. Schmidt, *Chem. Mater.* **2017**, *29*, 5182.
[19] P. C. Shih, J. Kim, C. J. Sun, H. Yang, *ACS Appl. Energy Mater.* **2018**, *1*, 3992.
[20] B. J. Kim, H. Jin, S. J. Moon, J. Y. Kim, B. G. Park, C. S. Leem, J. H. Park, *Phys. Rev. Lett.* **2008**, *101*, 076402.
[21] Q. Cui, J. G. Cheng, W. Fan, A. E. Taylor, S. Calder, M. A. McGuire; Y. Y. Jiao, *Phys. Rev. Lett.* **2016**, *117*, 176603.
[22] Y. Tokiwa, J. J. Ishikawa, S. Nakatsuji, P. Gegenwart, *Nat. Mater.* **2014**, *13*, 356.
[23] K. Ueda, T. Oh, B. J. Yang, R. Kaneko, J. Fujioka, N. Nagaosa, Y. Tokura, *Nat. Commun.* **2017**, *8*, 15515.
[24] H. B. Zhang, K. Haule, D. Vanderbilt, *Phys. Rev. Lett.* **2017**, *118*, 026404.
[25] K. Ueda, J. Fujioka, Y. Tokura, *Phys. Rev. B* **2016**, *93*, 245120.
[26] K. Matsuhira, M. Wakeshima, Y. Hinatsu, S. Takagi, *J. Phys. Soc. Jpn.* **2011**, *80*, 094701.
[27] S. Zhou, X. Miao, X. Zhao, C. Ma, Y. Qiu, Z. Hu, J. Zeng, *Nat. Commun.* **2016**, *7*, 11510.
[28] T. Hasegawa, N. Ogita, K. Matsuhira, S. Takagi, M. Wakeshima, Y. Hinatsu, M. Udagawa, *J. Phys.: Conf. Ser.* **2010**, *200*, 012054.
[29] K. Taniguchi, T. Katsufuji, S. Iguchi, Y. Taguchi, H. Takagi, Y. Tokura, *Phys. Rev. B* **2004**, *70*, 100401.
[30] J. K. Kawasaki, M. Uchida, H. J. Paik, D. G. Schlom, K. M. Shen, *Phys. Rev. B* **2016**, *94*, 121104.
[31] H.-D. Kim, H.-J. Noh, K. H. Kim, S.-J. Oh, *Phys. Rev. Lett.* **2004**, *93*, 126404.
[32] K. Xu, P. Chen, X. Li, Y. Tong, H. Ding, X. Wu, Y. Xie, *J. Am. Chem. Soc.* **2015**, *137*, 4119.
[33] X. Zhao, H. Zhang, Y. Yan, J. Cao, X. Li, S. Zhou, J. Zeng, *Angew. Chem., Int. Ed.* **2017**, *56*, 328.
[34] A. Grimaud, W. T. Hong, Y. Shao-Horn, J.-M. Tarascon, *Nat. Mater.* **2016**, *15*, 121.
[35] J. T. Mefford, X. Rong, A. M. Abakumov, W. G. Hardin, S. Dai, A. M. Kolpak, K. J. Stevenson, *Nat. Commun.* **2016**, *7*, 11053.
[36] A. Grimaud, O. Diaz-Morales, B. Han, W. T. Hong, Y. L. Lee, L. Giordano, Y. Shao-Horn, *Nat. Chem.* **2017**, *9*, 2695.
[37] A. Grimaud, K. J. May, C. E. Carlton, Y. L. Lee, M. Risch, W. T. Hong, Y. Shao-Horn, *Nat. Commun.* **2013**, *4*, 2439.
[38] J. Suntivich, W. T. Hong, Y. L. Lee, J. M. Rondinelli, W. Yang, J. B. Goodenough, Y. Shao-Horn, *J. Phys. Chem. C* **2014**, *118*, 1856.
[39] W. J. Kim, S. Y. Kim, C. H. Kim, C. H. Sohn, O. B. Korneta, S. C. Chae, T. W. Noh, *Phys. Rev. B* **2016**, *93*, 045104.
[40] C. R. Serrao, J. Liu, J. T. Heron, G. Singh-Bhalla, A. Yadav, S. J. Suresha, A. Vishwanath, *Phys. Rev. B* **2013**, *87*, 085121.